Geophysical Journal International

Geophys. J. Int. (2010) **181,** 1713–1724 doi: 10.1111/j.1365-246X.2010.04593.x

Earthquake detection capability of the Swiss Seismic Network

K. Z. Nanjo,[1,2] D. Schorlemmer,[3] J. Woessner,[2] S. Wiemer[2] and D. Giardini[2]

[1] *Earthquake Research Institute, University of Tokyo,* 1-1-1 *Yayoi, Bunkyo-ku, Tokyo* 113-0032, *Japan. E-mail: nanjo@eri.u-tokyo.ac.jp*
[2] *Swiss Seismological Service, ETH Zürich, Sonneggstrasse 5, Zürich* 8092, *Switzerland*
[3] *Southern California Earthquake Center, University of Southern California,* 3651 *Trousdale Parkway,* MC-0740, *Los Angeles,* CA 90089, *USA*

Accepted 2010 March 9. Received 2010 January 18; in original form 2009 May 12

SUMMARY

A reliable estimate of completeness magnitudes is vital for many seismicity- and hazard-related studies. Here we adopted and further developed the Probability-based Magnitude of Completeness (PMC) method. This method determines network detection completeness (M_P) using only empirical data: earthquake catalogue, phase picks and station information. To evaluate the applicability to low- or moderate-seismicity regions, we performed a case study in Switzerland. The Swiss Seismic Network (SSN) at present is recording seismicity with one of the densest networks of broad-band sensors in Europe. Based on data from 1983 January 1 to 2008 March 31, we found strong spatio-temporal variability of network completeness: the highest value of M_P in Switzerland at present is 2.5 in the far southwest, close to the national boundary, whereas M_P is lower than 1.6 in high-seismicity areas. Thus, events of magnitude 2.5 can be detected in all of Switzerland. We evaluated the temporal evolution of M_P for the last 20 yr, showing the successful improvement of the SSN. We next introduced the calculation of uncertainties to the probabilistic method using a bootstrap approach. The results show that the uncertainties in completeness magnitudes are generally less than 0.1 magnitude units, implying that the method generates stable estimates of completeness magnitudes. We explored the possible use of PMC: (1) as a tool to estimate the number of missing earthquakes in moderate-seismicity regions and (2) as a network planning tool with simulation computations of installations of one or more virtual stations to assess the completeness and identify appropriate locations for new station installations. We compared our results with an existing study of the completeness based on detecting the point of deviation from a power law in the earthquake-size distribution. In general, the new approach provides higher estimates of the completeness magnitude than the traditional one. We associate this observation with the difference in the sensitivity of the two approaches in periods where the event detectability of the seismic networks is low. Our results allow us to move towards a full description of completeness as a function of space and time, which can be used for hazard-model development and forecast-model testing, showing an illustrative example of the applicability of the PMC method to regions with low to moderate seismicity.

Key words: Probability distribution; Seismicity and tectonics; Seismic attenuation; Computational seismology; Statistical seismology; Europe.

1 INTRODUCTION

Earthquake catalogues are one of the primary products of seismology. The process to create such catalogues is complex. Examples involved in the process include detection of phases by seismic stations, their interpretation as earthquake signals and a calibrated location and magnitude determination. Catalogues inherently depend on the detection capability of seismic networks, which is related to the distribution, density and characteristics of individual stations, their local site and noise conditions, processing software and processing strategies. One commonly used parameter to characterize the recording capability of a network is the magnitude of completeness (M_c), understood as the magnitude above which earthquakes are recorded with a certain probability close to 1.

A detailed knowledge of the space and time variations of M_c is critical for many earthquake-hazard or earthquake-physics studies because they evaluate statistical properties of microseismicity. Such evaluations can only be meaningful if the samples of the catalogues contain complete recordings of sets of microseismicity. For example, studies of earthquake-size distributions or seismicity rates are highly dependent on the knowledge of M_c (e.g. Wiemer & Wyss 2002; Schorlemmer *et al*. 2005).

Various approaches have been published on the determination of M_c and reviews of various techniques are given by Woessner & Wiemer (2005) and Schorlemmer & Woessner (2008). Recently, a new method called Probability-based magnitude of completeness (PMC) was proposed by Schorlemmer & Woessner (2008). This method estimates detection probabilities $P_E(M, \boldsymbol{x}, t)$ for given magnitudes M and probability-based magnitudes of completeness $M_P(\boldsymbol{x}, t)$ at locations $\boldsymbol{x}$ for the time t. PMC treats the completeness as a function of recording capabilities of the seismic network and uses only empirical data, namely the phase-pick information, the stations' operational periods and the attenuation relation specifying the magnitude–distance dependency as used by the network to determine magnitudes M. PMC does not assume a model such as the Gutenberg–Richter (GR) relation (Gutenberg & Richter 1944), $\log_{10} N = a - bm$, where a and b are constants and N is the number of earthquakes with magnitudes $M \geq m$, whereas the methods of Wiemer & Wyss (2002) and Woessner & Wiemer (2005) assumed the GR model. Matsumura (1984), Papanastassiou & Matsumura (1987) and Morandi & Matsumura (1991) developed a method to estimate the parameters similar to $P_E(M, \boldsymbol{x}, t)$ and $M_P(\boldsymbol{x}, t)$ for central Japan. Independently from these works, Schorlemmer & Woessner (2008) developed PMC and applied it to southern California.

In this paper, we evaluate the detection performance of the Swiss Seismic Network (SSN) applying the PMC method. The SSN produces the official earthquake catalogue for Switzerland (Fig. 1), a region with moderate seismic activity. Our work extends a preliminary analysis by Bachmann *et al.* (2005), who implemented a first version of PMC for Swiss data. The major difference between Bachmann *et al.* (2005) and this study is that we derive detection–probability distributions for each station depending on the phase picks of each station as proposed by Schorlemmer & Woessner (2008) whereas Bachmann *et al.* (2005) computed one average detection–probability distribution for all stations, by stacking phase picks from all stations. To extend the PMC method, we introduce an approach for assessing the uncertainty, $\sigma_P(\boldsymbol{x}, t)$, of $M_P(\boldsymbol{x}, t)$ based on a bootstrap method (Efron 1979). In addition, we show how PMC can be used as network planning tool by adding virtual stations to the SSN to simulate detection probabilities. Further, we compare the PMC approach with a GR-based approach. For the latter, we compute M_c by using the entire-magnitude range (EMR) method [$M_{c(EMR)}$] (Woessner & Wiemer 2005), a modified version from a method introduced by Ogata & Katsura (1993). In addition to detection capabilities parameterized by $P_E(M, \boldsymbol{x}, t)$ and $M_P(\boldsymbol{x}, t)$, we make an attempt to estimate the number of missing events as an alternative expression of earthquake detectability. Our study provides for the first time a comprehensive spatio-temporal completeness analysis for Switzerland as a baseline for future seismicity- and hazard-related studies.

2 METHOD

PMC relies on the analysis of empirical data (see Schorlemmer & Woessner 2008 for details): (1) station data describing location and on-/off-times (the dates when the station operation was started and terminated, respectively) for each station in the network, (2) the earthquake catalogue describing location, time and magnitude M for each event including phase-pick data describing which stations recorded (picked) each event's P-wave arrivals and (3) the attenuation relation used for magnitude determination.

The method is divided into an analysis and a synthesis part. In the analysis, we first compile for each station data triplets containing, for each earthquake that occurred during the station's operational periods, the information on whether P phases were picked or not, the magnitude M of the event and its distance L from the station. Fig. 2(a) shows an example of the triplets from station SENIN. Using the triplets and the attenuation relation, we derive for each station a distribution of detection probabilities $P_D(M, L)$, see Schorlemmer & Woessner (2008). According to the procedure outlined in Schorlemmer & Woessner (2008), we determine smoothed station detection–probability distributions.

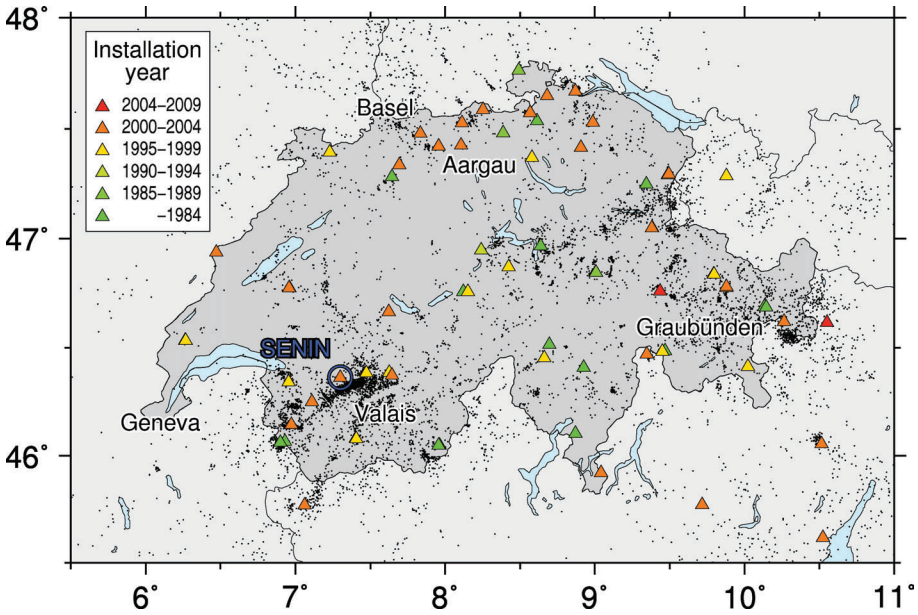

Figure 1. Location map of seismograph stations (triangles) and earthquakes (circles) in and around Switzerland. Station colours indicate installation times. Station SENIN is highlighted; a broad-band three-component seismograph in operation since 2002 February 26 at the location of 7.299°E and 46.363°N, and elevation of 2035 m. Swiss borders are shown in thick solid curves. Geographical references are included.

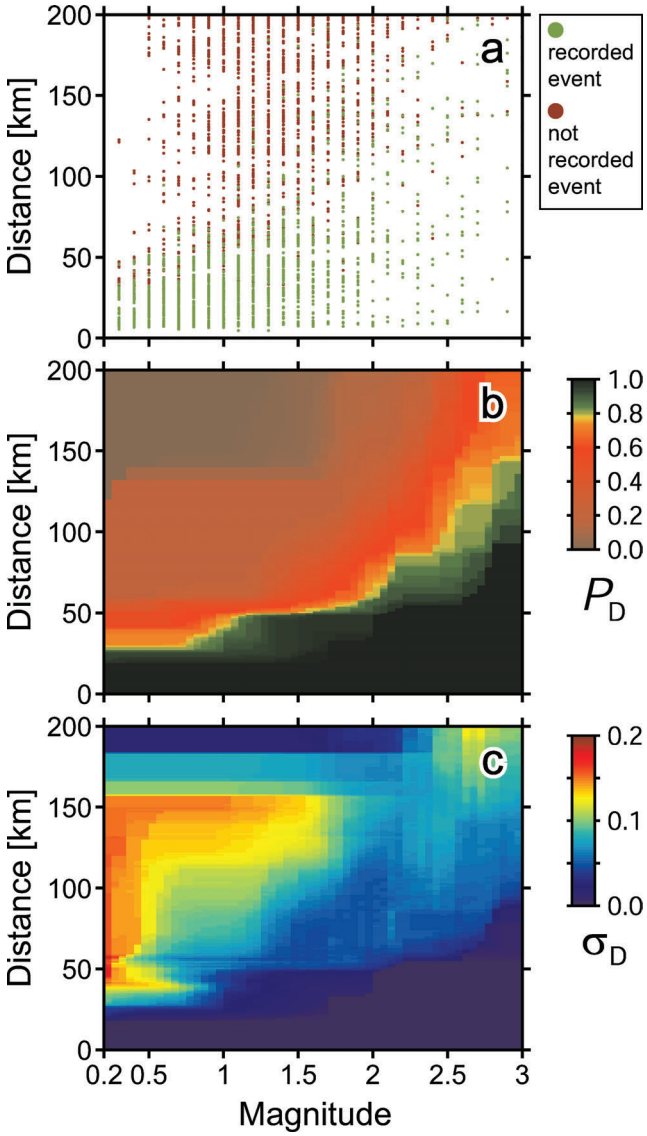

Figure 2. Detection characteristic of station SENIN, highlighted in Fig. 1. (a) Distribution of 1890 not picked (red) and 1958 picked (green) events for the station. (b) detection–probability distribution, P_D. (c) distribution of uncertainties of P_D, σ_D.

In the synthesis part, basic combinatorics is used to obtain detection probabilities $P_E(M, \boldsymbol{x}, t)$ for detecting an earthquake of M at a location $\boldsymbol{x}$ (Figs 3a and b), given the specific network configuration at the time t. $P_E(M, \boldsymbol{x}, t)$ is the probability that four or more stations have recorded the P wave of an earthquake with M at $\boldsymbol{x}$ for t. This minimum number of stations must be adjusted to the triggering algorithm if it requires a different number of stations with a possible phase signal to initiate the location procedure, or if S-wave picks play a significant role in triggering the location procedure. The completeness magnitude $M_P(\boldsymbol{x}, t)$ is given as the magnitude M above which earthquakes are detected with $P_E(M, \boldsymbol{x}, t) \geq 1 - Q$, where Q is the complementary probability that events will be missed (Schorlemmer & Woessner 2008). The choice of the Q value is arbitrary and should reflect desired accuracy. We take $Q = 0.0001$ for conservative estimates.

The results obtained in this paper are only valid in the absence of strong seismic clustering such as large aftershock sequences. During aftershock clustering, completeness values are higher than those at times of background seismicity (e.g. Bachmann *et al.* 2005, 2007; Woessner & Wiemer 2005; Nanjo *et al.* 2007). Because our completeness is based on all seismicity including aftershocks and normal background events, it underestimates for the periods of strong seismic clustering. The users should be aware of such temporal changes in the completeness when they analyse aftershock sequences.

We adopt a bootstrap approach for generating uncertainty estimates of M_P. For each station, we bootstrap our basic input data, the data triplets. We resample all triplets with replacement, where the number of events re-sampled is the same as the number of events in the original sample. We apply this bootstrapping method to all stations. From $P_D(M, L)$ based on bootstrapped triplets for stations operating at time t, we calculate $P_E(M, \boldsymbol{x}, t)$ and then $M_P(\boldsymbol{x}, t)$. We iterate N_B times (here $N_B = 300$), so that we obtain N_B values of $M_P(\boldsymbol{x}, t)$, from which we compute the standard deviation $\sigma_P(\boldsymbol{x}, t)$ (Fig. 3d). We performed the computation for an increasing number of bootstrap samples, starting at $N_B = 100$ bootstrap samples as a preliminary analysis and find results to stabilize at about $N_B = 200$. For the sake of brevity, we further use P_D, P_E, M_P and σ_P instead of $P_D(M, L)$, $P_E(M, \boldsymbol{x}, t)$, $M_P(\boldsymbol{x}, t)$ and $\sigma_P(\boldsymbol{x}, t)$, respectively.

Fig. 2(c) shows the uncertainty, σ_D, for the station SENIN. σ_D is mainly in the range of 0 to 0.2. High uncertainties of $\sigma_D > 0.1$ fall in sparse data areas of the distribution in Fig. 2(a) with low probabilities of $P_D < 0.8$ (Fig. 2b), whereas low uncertainties of $\sigma_D < 0.1$ are associated with denser data and with high probabilities $P_D > 0.8$. Accordingly, σ_D patterns were obtained for other stations of the SSN. These uncertainty estimates do not include assumptions about the magnitude uncertainties in the magnitude determination process.

In addition to network detection capabilities indicated by P_E, M_P and σ_P, seismologists may be interested in the number of undetected (missing) events for a region of interest. To obtain this number for magnitude M, we consider detected (catalogued) earthquakes of the same M. The total number of detected earthquakes of M for the interest region is denoted by $n^d_{tot}(M) \equiv n^d_{tot}$. We divide the interest region into subregions, each centred at $\boldsymbol{x}$ with area denoted by $A(\boldsymbol{x})$. The number of detected (catalogued) earthquakes of M for a subregion at $\boldsymbol{x}$, $n^d(M, \boldsymbol{x}) \equiv n^d$, is used to obtain the number of undetected events of M, $n^u(M, \boldsymbol{x}) \equiv n^u$. If one or more earthquakes are found in the subregion, this number is assigned to n^d. If not, a positive and <1 small quantity must be assigned to n^d. Although a fundamental problem is how to assign it, as an approximation we use the information on the most neighbouring earthquake to the location $\boldsymbol{x}$, as follows: (1) we consider the distance of the nearest earthquake to $\boldsymbol{x}$, $r_n(M, \boldsymbol{x}) \equiv r_n$; (2) the area $A(\boldsymbol{x})$ is divided by πr_n^2 to compute the assumed number of events for a subregion at $\boldsymbol{x}$, $n_a(M, \boldsymbol{x}) \equiv n_a$ $(= A(\boldsymbol{x})/\pi r_n{}^2 < 1)$; (3) we assign n_a to n^d and (4) we do the same (1–3) for all subregions. Because of the assignment for subregions without earthquake, the sum of n^d over all subregions for M, denoted by $N^d(M) \equiv N^d$, is larger than n^d_{tot}. Thus n^d is normalized by N^d/n^d_{tot} to equate N^d with n^d_{tot}. Using the normalized value, $n^d n^d_{tot}/N^d$, we compute n^u for a subregion at $\boldsymbol{x}$, using the following equation $n^u = (n^d n^d_{tot}/N^d)((1–P_E)/P_E)$. The sum of n^u over all subregions gives the total number of undetected (missing) events in the study region for M, $n^u_{tot}(M) \equiv n^u_{tot}$. This attempt explores the possible use of PMC as a tool to estimate the number of missing earthquakes in moderate-seismicity regions.

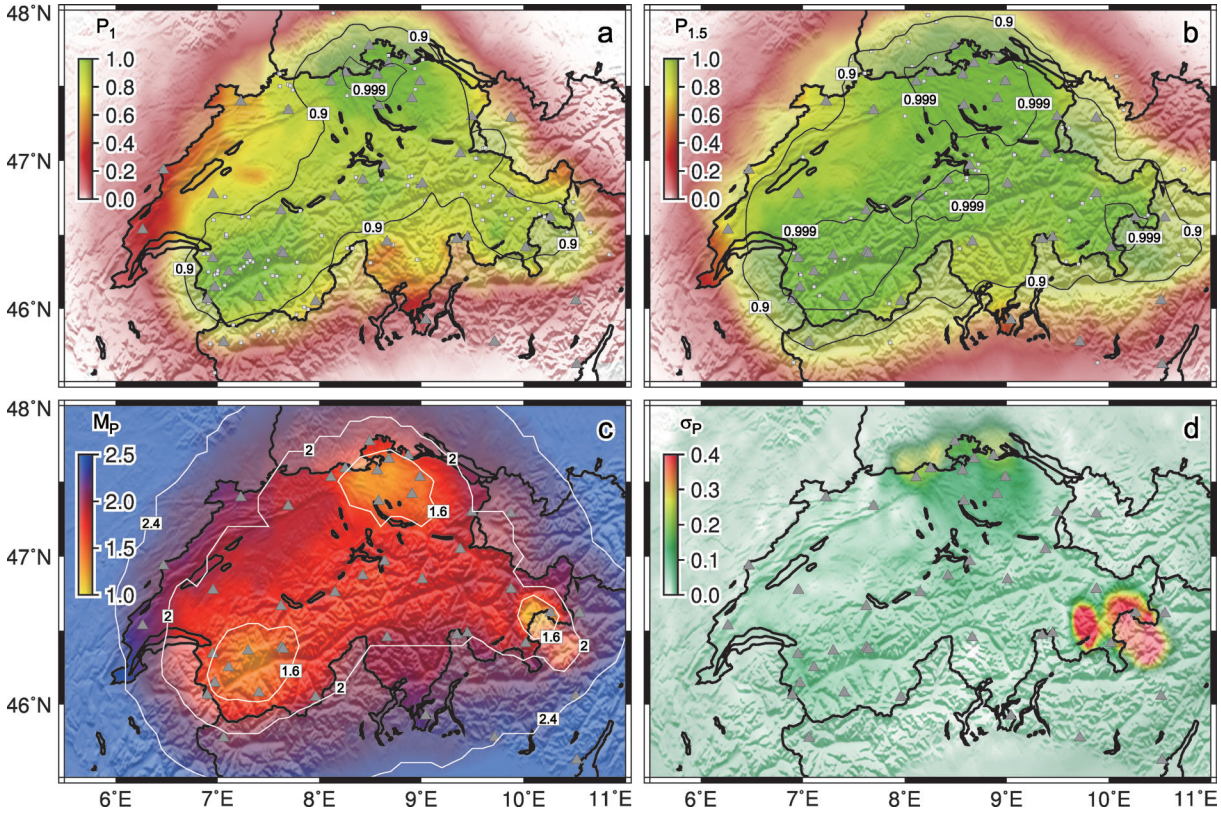

Figure 3. Maps of network-detection probabilities. (a) $P_1 = P_E|_{M=1}$ and (b) $P_{1.5} = P_E|_{M=1.5}$ for the stations (marked as triangles) in operation on 2008 April 1. Grey squares mark earthquakes of respective magnitude that were recorded in the previous two years. Black lines show contours of $P_E = 0.9$ and 0.999. (c) map of probability-based completeness, M_P, for the same day and set of stations. White lines show contours for $M_P = 1.6$, 2.0 and 2.4. (d) map of uncertainties of M_P, σ_P.

3 DATA

We analyse data of the SSN, operated by the Swiss Seismological Service [Schweizerischer Erdbebendienst, SED]. This network continuously monitors the ongoing earthquake activity, aiming to detect all earthquakes down to magnitude 1 or below (e.g. Baer *et al.* 2005). The SED is recording seismicity in and around Switzerland with one of the densest networks of broad-band sensors in Europe with an average station separation of about 20 km. A digital acquisition system has replaced the use of analogue short-period sensors in the period 1998–2002 (Baer *et al.* 2005). To cover the extent of the SSN (Fig. 1), we define the study region as the box 5.5–11.0°E and 45.5–48.0°N. Because P_E, M_P and σ_P are computed for points in space and time, we have to define the depth for which we compute these values. To find a meaningful depth, we investigate the depth distribution of earthquakes in Switzerland. The mean and the standard deviation for events within the box 5.5–11.0°E and 45.5–48.0°N are 7.4 and 4.1 km, respectively. 97 per cent of all earthquakes have shallower depths than 20 km. We compute P_E, M_P and σ_P at the depth 7.5 km, roughly the mean depth of events. We use the earthquake catalogue of the SSN (http://histserver.ethz.ch) from 1983 January 1 to 2008 March 31, which includes earthquakes in Switzerland and bordering countries. We do not cut the catalogue before generating the detection–probability distributions P_D. The information about the permanent stations, the phase information for each earthquake in the catalogue and the attenuation relation are obtained from the SED. The earthquake catalogue contains 21 414 events with 285 953 *P*-phase determinations.

We use *P*-phase information only, because the triggering algorithm of the SSN requires the detection of four *P* phases. To improve the reliability of the automatic location of earthquakes at the periphery and outside of Switzerland, the SED implemented in 2002 an automatic system for retrieving data from foreign stations (Baer *et al.* 2005). The foreign stations that are connected to the triggering algorithm are included in our analysis. The SED routinely computes local magnitudes M_L with the attenuation relationship: $M_L = \log A_{EA} - \log A_0$, where A_{EA} is the equivalent amplitude in millimetres of a Wood–Anderson seismograph and A_0 accounts for distance attenuation with $\log A_0 = -0.018\ D - 1.77$ for hypocentral distances $D \leq 60$ km and $\log A_0 = -0.0038\ D - 2.62$ for 60 km $< D <$ 700 km (Kradolfer 1984; Braunmiller *et al.* 2005). This equation is used to convert raw data triplets (Fig. 2a) to detection probabilities P_D (Fig. 2b) as described by Schorlemmer & Woessner (2008). Magnitude determination is consistent throughout the magnitude range in which we are interested for Switzerland.

4 RESULTS

4.1 Sensitivity checks on anisotropy and depth dependence of station probability distributions

We first perform simple sensitivity checks on anisotropy and depth dependence of detection capabilities of stations. We separately consider events located in the northeast/southwest (NE/SW) and in the northwest/southeast (NW/SE) quadrants of the station. Figs 4(a) and

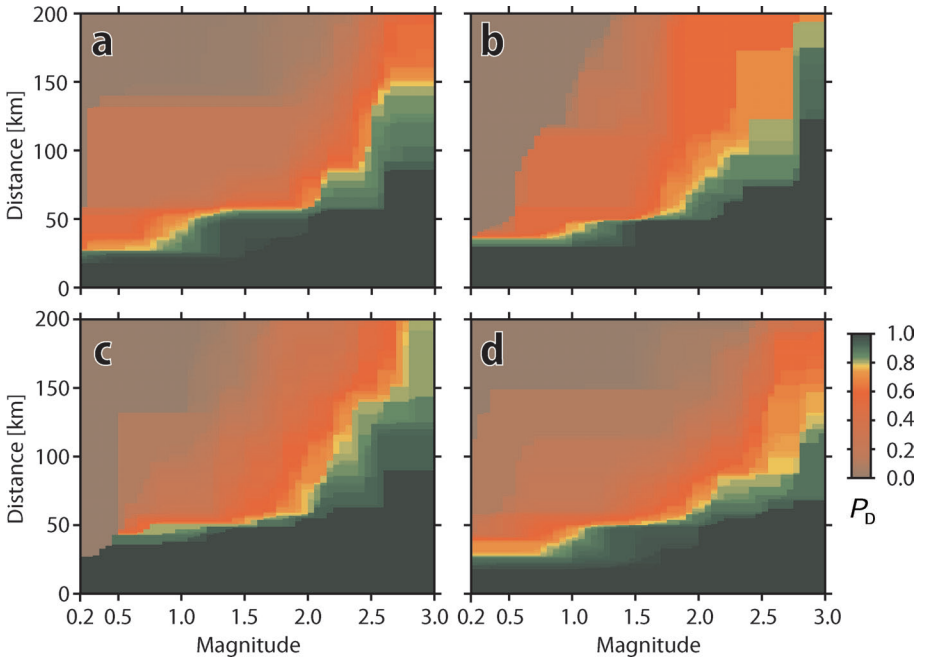

Figure 4. Distribution of detection probabilities, P_D, for station SENIN. (a) and (b) show the cases for using events situated in the northeast/southwest (NE/SW) and the northwest/southeast (NW/SE) quadrants of the station, respectively. (c) indicates the case for using events with depths shallower than or equal to 7.5 km. The case in (d) is based on events with depths deeper than 7.5 km.

(b) show the distribution of P_D for station SENIN for the NE/SW and NW/SE quadrants, respectively. The distributions of P_D for earthquakes with depths less or equal than 7.5 km is given in Fig. 4(c) and deeper events are used to create Fig. 4(d). General patterns of P_D in Figs 4(a)–(d) are similar to those in Fig. 2(b). We make the same observation for other stations in the network. In Switzerland, a region with moderate seismicity, there was no significant seismic clustering that can disturb the homogeneous input triplets. Thus, the PMC method for Switzerland provides stable estimates of P_D, even if the above input-data conditions change, and these estimates are not sensitive to anisotropy and do not show any depth dependence. Because of this insensitivity, our mapping of network-detection capabilities, indicated by P_E, M_P and σ_P, is based on one station probability, P_D, for each station, estimated from all available events.

4.2 Mapping detection probabilities, completeness magnitude and uncertainty

We present maps of detection probabilities, P_E, for specific magnitudes, a map of magnitude of completeness, M_P and a map of its uncertainty, σ_P, for 2008 April 1. The number of stations of the SSN operating at this day is 38. Additionally, 16 foreign stations, 2 stations of the network of Zentralanstalt für Meteorologie und Geodynamik (ZAMG) from Austria and 14 Italian stations under the Bozen network and the network of the Istituto Nationale di Geofisica e Vulcanologia (INGV) are considered as they are included in the SED triggering system.

We examine the spatial distribution of detection probabilities P_E for $M = 1.0$ and 1.5 at 2008 April 1 (Figs 3a and b). We use a grid spacing of $0.05^\circ \times 0.05^\circ$ and compute P_E at a depth of 7.5 km. As expected, the two maps show that P_E increases with M. Earthquakes of $M = 1.0$ and 1.5 during the period 2006 April 1–2008 April 1 were detected in areas with predominantly high respective detection probabilities (Figs 3a and b), showing consistency between our synthesis and the observation. Figs 3(a) and (b) show strong spatial variability of detection probabilities: large P_E for $M = 1.0$ highlights in parts of the cantons Aargau and Valais. P_E for $M = 1.0$ in the border region from Geneva to Basel is comparatively low due to a lack of reporting stations in France. This affects the lower Rhine Graben around the city of Basel, the region that experienced the largest historically known earthquake in central Europe ($M \approx 6.5$–6.9) in 1356 (Fäh *et al.* 2003). Although $P_E(M = 1.5, \boldsymbol{x}, t)$ values in Fig. 3(b) are generally well above 0.9 in almost all over the country, we again see a similar variability and a strong decrease towards the border to France.

We found M_P for 2008 April 1 to vary between 1.1 and 2.5 within Switzerland (Fig. 3c). M_P values are below 1.6 in parts of the cantons Valais, Aargau and Graubünden. In other areas, M_P values are generally between 1.6 and 2.4 with the highest value of 2.5 at the westernmost tip of Switzerland in Geneva. Except for Graubünden, M_P reaches values of about 1.8–2.4 in the border regions. This results from the sparser station coverage caused by the limited number of foreign stations feeding data in real time to the SED. Low M_P values in Graubünden are associated with the station MOSI (10.55°E, 46.62°N) operated by the Bozen network, which was installed close to the border and integrated into the SSN on 2006 November 1 (Fig. 5, last two frames). Animation S1 (see Supporting Information) also shows the decrease of M_P in Graubünden after the installation of this station. In summary, the SED network with its current configuration is capable of detecting all earthquakes of $M \geq 2.5$ in Switzerland. In some regions, the completeness magnitude is as low as $M_P < 1.6$.

In Fig. 3(d), we plot a map of one standard deviation, σ_P, for $t =$ 2008 April 1. σ_P ranges from 0 to 0.4, with the large majority of values being less than 0.1. High uncertainties in Graubünden are associated with the station MOSI. The number of triplets used

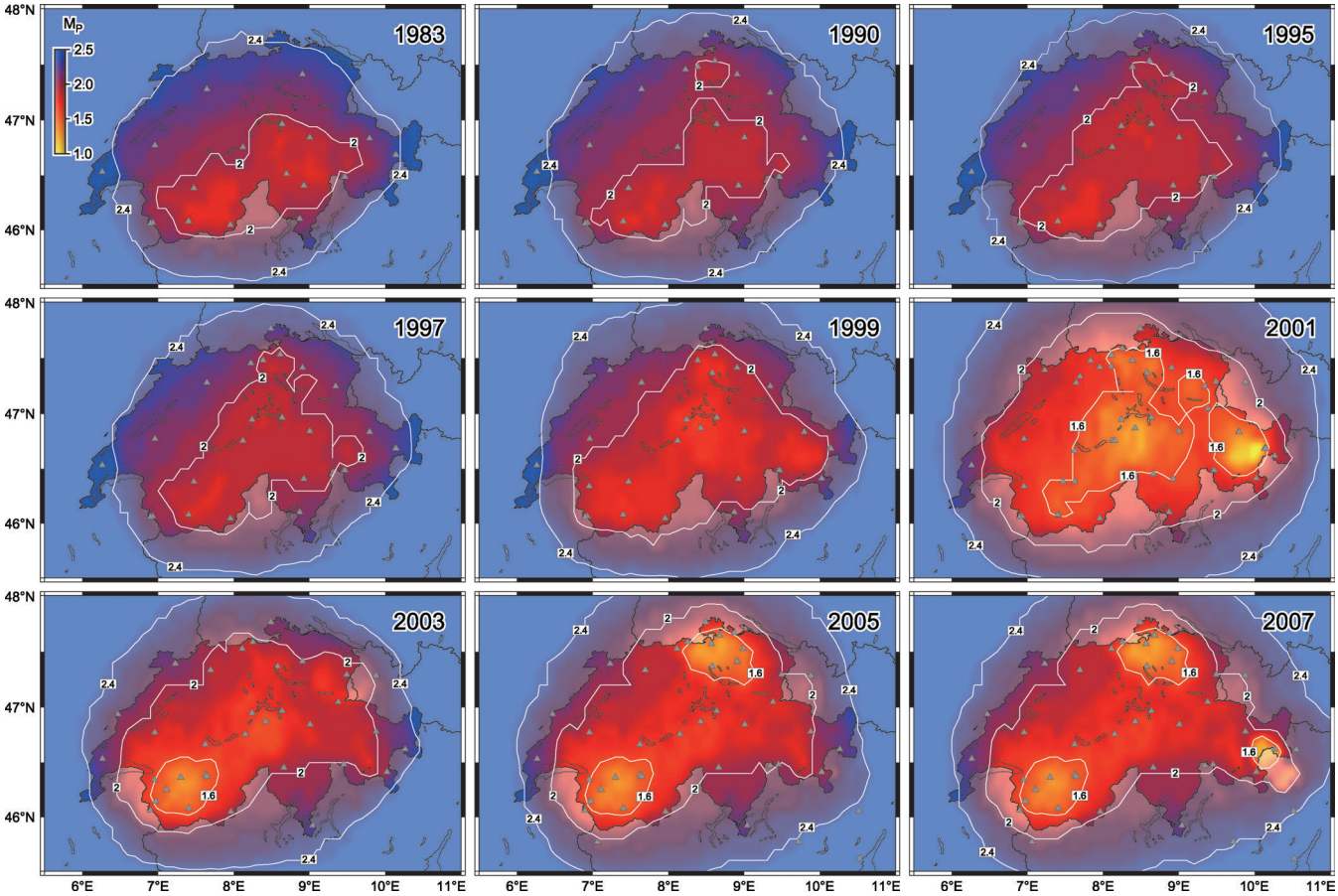

Figure 5. Maps of probability-based magnitude of completeness, M_P, for different points in times. All maps show M_P at January 1 of the respective year as indicated in the frames (1983, 1990, 1995, 1997, 1999, 2001, 2003, 2005 and 2007). White lines show contours for $M_P = 1.6$, 2.0 and 2.4.

to compute P_D values of the station is small (107 picked and 289 not picked events occurred during the operational period of this station) because it was installed only recently (2006 November 1). The probabilities P_D for station MOSI are influenced more by the bootstrapping than that for other stations. Thus the bootstrapping affects M_P estimates in that area more strongly so that σ_P estimates are high in Graubünden, which reflects correctly the limited knowledge about the performance of station MOSI.

From 1998 to 2002, the configuration of the SSN fundamentally changed (e.g. Baer *et al.* 2005). To demonstrate the network improvements, we show the spatio-temporal evolution of M_P in Fig. 5 and Animation S1. Fig. 5 shows sequential snapshots on January 1 for the years 1983, 1990, 1995, 1997, 1999, 2001, 2003, 2005 and 2007. The detection level improved from an average of $2.0 \leq M_P \leq 2.4$ in the 1990s to completeness values between $1.1 \leq M_P \leq 2.4$ in 2008 (Fig. 3c). Note that the detection capabilities in 2001 were better than the capabilities after 2003 in Graubünden. This is due to the fact, that the network installed by the end of 2002 was initially operated in combination with the short-period stations; once the new system demonstrated its reliability, most of the short-period stations were decommissioned. Nonetheless, at many locations, M_P values improved after 2003 (Figs. 3c, 5) following the current completion of the network. The modernization of the network resulted in a significant improvement of the overall detection capability. See also Animation S1, which shows the spatio-temporal evolution of completeness.

4.3 Estimating undetected events

To consider undetected (missing) events, we use detected (catalogued) earthquakes in the two-year period from 2006 April 1 to 2008 April 1, same as the period used for events shown in Figs 3(a) and (b). As a subregion centred at $\boldsymbol{x}$, we use a box of size of 0.05° in latitude and longitude. We compute the number of undetected events of magnitude M, n^u, for each box with $P_E = P_E(M, \boldsymbol{x}, t)$ for $t =$ 2008 April 1. Figs 6(a) and (b) show n^u for $M = 1.0$ and 1.5, respectively. As expected, Fig. 6 shows that n^u in regions far outside of the Swiss territory is quite high because of the outside of the SSN. For meaningful discussion on n^u and n^u_{tot}, we reduce such outside regions. We define a region smaller than the original study region: 6.0–10.5°E and 45.8–47.8°N. n^u for $M = 1.0$ is less than 1 for almost all boxes. Comparison with Fig. 3(a) shows that relatively high n^u values are observed at locations where earthquakes are detected and P_E values are close to 0.9 or below, and at the corners of the study region where P_E is pretty close to 0 and there is no detected earthquake. Similarly n^u for $M = 1.5$ is smaller than or equal to 1 in all over the country. Although n^u for $M = 1.5$ is generally smaller than n^u for $M = 1.0$, comparison between Figs 3(b) and 6(b) shows that a correlation for $M = 1.5$ among n^u, P_E and detected events is similar to that for $M = 1.0$. The total number of undetected earthquakes in the study region for 2006–2008 is $n^u_{tot} = 24.6$ and 5.8 for $M = 1.0$ and 1.5, respectively. To compare in n^u_{tot} among M values, n^u_{tot} is given in the inset as a function of M. n^u_{tot} generally increases with the decrease of M: n^u_{tot} varies

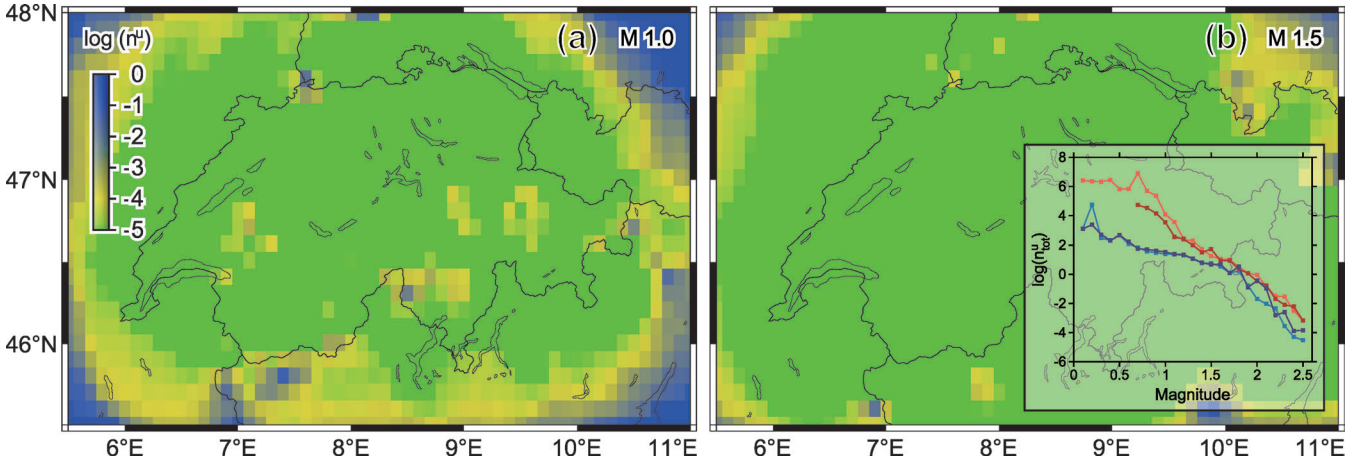

Figure 6. Maps of the number of undetected events, n^{u}, for (a) $M = 1.0$ and (b) $M = 1.5$ at $t =$ 2008 April 1. The inset shows the total number of undetected events, $n^{\mathrm{u}}_{\mathrm{tot}}$, as a function of M for the four periods: 2006 April 1–2008 April 1 (light blue), 2004 January 1–2006 January 1 (dark blue), 1993 January 1–1995 January 1 (dark red) and 1988 January 1–1990 January 1 (light red). For the period 1993 January 1–1995 January 1, no data for magnitudes below 0.6 are shown because no earthquake was recorded in the corresponding period. Data for the former two periods are coloured in blue, showing examples from post-SSN modernization. The latter two (red) are representatives before the modernization.

between 2.9×10^{-5} for $M = 2.5$ and 5.8×10^{4} for $M = 0.2$. This shows that smaller earthquakes are more frequently undetected than larger ones are. To incorporate the history of SSN, we take three 2-yr periods: 2004 January 1–2006 January 1, 1993 January 1–1995 January 1 and 1988 January 1–1990 January 1. The first period is an example from the post-SSN modernization whereas the latter two are representatives before the start of the SSN modernization. The magnitude-dependent $n^{\mathrm{u}}_{\mathrm{tot}}$ behaviour for these periods is included in the inset. We again see a negative correlation between $n^{\mathrm{u}}_{\mathrm{tot}}$ and M, similar to for the period 2006–2008. Further, we find that $n^{\mathrm{u}}_{\mathrm{tot}}$ before the network modernization is larger for most magnitudes than $n^{\mathrm{u}}_{\mathrm{tot}}$ after it, with larger differences in $n^{\mathrm{u}}_{\mathrm{tot}}$ for smaller magnitudes. This demonstrates the variability of detection threshold: the more the SSN is modernized, the higher the detection of microearthquakes is. We attempt to show an alternative to express network-detection capabilities.

4.4 Virtual installation of stations

To infer the effect of adding station(s) to the SSN on the completeness magnitude M_{P}, we perform scenario computations by virtually placing additional stations to the current network configuration (2008 April 1). We compare the probability-based completeness magnitudes between the virtual case, M_{PV}, and the real case, M_{P}, for all locations $\boldsymbol{x}$ in the study region with a grid spacing of $0.05^{\circ} \times 0.05^{\circ}$: $\Delta M_{\mathrm{P}} = M_{\mathrm{P}} - M_{\mathrm{PV}}$. A fundamental problem is the definition of detection–probability distributions P_{D} to be used for individual stations installed for the virtual case. Such a distribution depends on station characteristics, local site and noise conditions. As an approximation, we assume that the probabilities P_{D} for a virtual station are the same as the probabilities for the station closest to the location of the virtual station. We argue for a best-case scenario because station locations were well prepared based on site-specific measurements for the modernized network. However, we are aware of the fact that the station characteristic may be very different because of local site conditions, and that for appropriate station planning additional geological data are necessary.

Figs 7(a)–(d) show ΔM_{P} for virtual station installations at different locations in addition to the existing network at 2008 April 1. The first four frames (a–d) show examples of installation of single stations of which the first three are expected future locations of stations for the SSN. In all cases, the installation would improve the detection capabilities in the surrounding regions by $\Delta M_{\mathrm{P}} > 0.1$. Depending on the location, the detection improvement varies from max $\Delta M_{\mathrm{P}} = 0.2$ in frame b to max $\Delta M_{\mathrm{P}} = 1.1$ in frame a. The spatial pattern of ΔM_{P} is complex and anisotropic. These patterns can be explained by different contributions of neighbouring stations with different detection–probability distributions. In any case, adding new stations is improving detection probabilities of the network.

Figs 7(d)–(f) show the case of increasing number of stations installed at locations close to each other. This demonstrates that densely located stations enhance detectability of earthquakes for the corresponding site: the max ΔM_{P}-value in (d), (e) and (f) is 0.4, 1.1 and 1.2 for one, two and three stations, respectively. This computation shows a similar effect as the scenario computation in Schorlemmmer & Woessner (2008), where the local Anza network significantly increases detectability of microearthquakes in the Anza region.

4.5 Comparison between EMR and PMC approaches

PMC introduces a new method to determine the detection threshold of a network and has been applied to networks in California (Schorlemmer & Woessner 2008; Bachmann *et al.* 2007) and Italy (Schorlemmer *et al.* 2010), whereas assessing M_{c} using traditional GR-based methods has been applied in many studies. We perform a comparison between the results of both methods and address the fundamental question if PMC and GR-based methods provide similar results.

The EMR method (Woessner & Wiemer 2005) estimates the completeness magnitude by fitting separately the complete and the incomplete parts of a given frequency–magnitude distribution. For earthquakes equal or above a certain magnitude (M_{cc}), the EMR method assumes the GR-law behaviour. Below M_{cc}, the method assumes a cumulative normal distribution. For increasing M_{cc} values, the EMR method computes the log likelihood to measure the fit of synthetic frequency–magnitude distribution models and the observed distribution for the EMR data. The completeness magnitude M_{C} is defined as $M_{\mathrm{C}} = M_{\mathrm{cc}}$ for which the maximum log-likelihood is obtained.

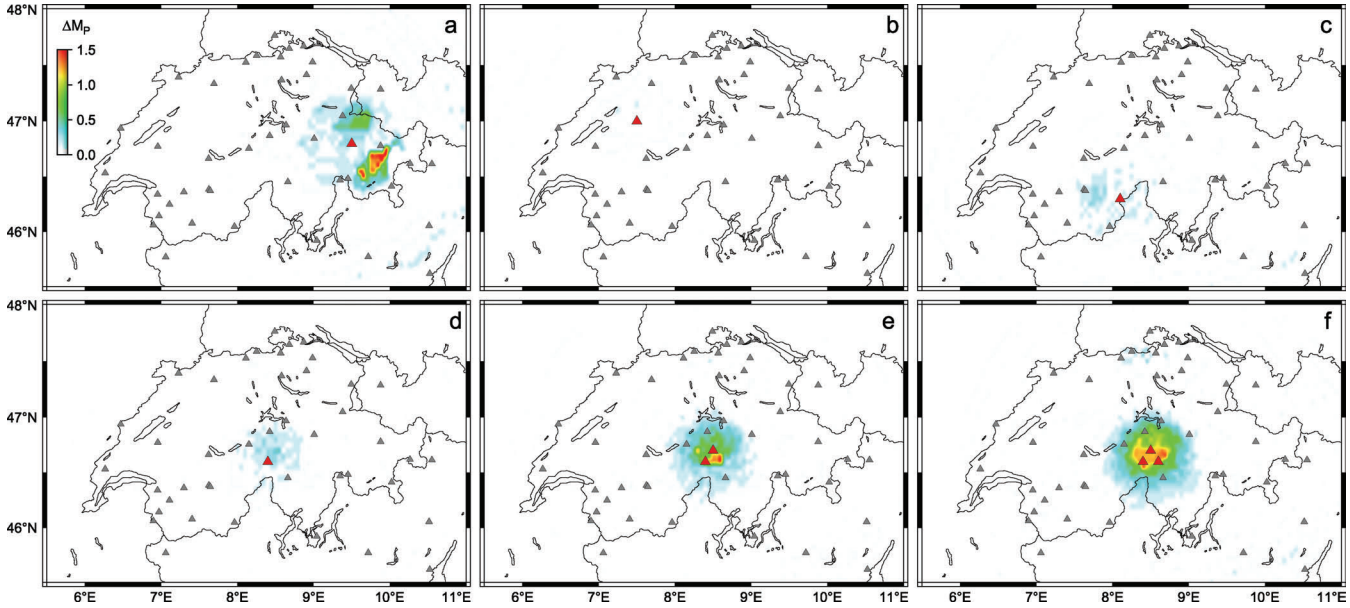

Figure 7. Scenario computations of adding virtual stations to the network to examine their effect on network detection capabilities. Virtual stations are added to the SSN in operation on 2008 April 1. The station locations are (a) 9.5°E/46.8°N, (b) 7.5°E/47.0°N, (c) 8.1°E/46.3°N, and (d) 8.4°E/46.6°N. (e) We added another station (8.5°E/46.7°N) to this configuration (d). (f) We added a third station (8.6°E/46.6°N). Colour coded is the difference in completeness magnitude between virtual case (M_{PV}) and real case (M_P) in Fig. 3. The detection–probability distribution, P_D, for each virtual station is the same as that for the closest real station.

We apply the EMR method to all events in the catalogue for the period from the start time $t_S = 1983$ January 1 to the end time $t_E = 2008$ March 31. The completeness magnitude, $M_{c(EMR)} \equiv M_{c(EMR)}(\boldsymbol{x}_c, t_S, t_E)$, and its uncertainty $\sigma_c \equiv \sigma_c(\boldsymbol{x}_c, t_S, t_E)$ are computed for points $\boldsymbol{x}_c$ in space. We collect earthquakes within a cylindrical volume of 20 km height and 30 km radius at points $\boldsymbol{x}_c$. We use a grid spacing of $0.1^\circ \times 0.1^\circ$ and perform 200 bootstrap runs for computing $M_{c(EMR)}$ and σ_c. The radius of these cylindrical volumes is large because the density of earthquakes in many regions is very low. If such a volume contains less than 80 earthquakes, no $M_{c(EMR)}$ and σ_c can be computed.

Completeness levels vary spatially throughout Switzerland between 1.3 and 2.2 (Fig. 8a). Insets in Fig. 8 show examples of frequency–magnitude distributions for four locations, 9.0°E/47.5°N, 7.5°E/46.5°N, 8.2°E/46.6°N and 7.4°E/46.9°N (points J, K, V and W in Figs 8a and b). The points J and K are representing regions of lower and higher seismicity, respectively. The highest uncertainty σ_c in Switzerland is obtained at V. Completeness $M_{c(EMR)}$ at point W is the highest in Switzerland and, only for this point, $M_{c(EMR)}$ is larger by 0.1 magnitude units than the completeness of the PMC approach. We obtain $M_{c(EMR)} \pm \sigma_c = 1.9 \pm 0.16$ at J and 1.4 ± 0.16 at K, 1.7 ± 0.31 at V and 2.2 ± 0.28 at W. Completeness values increase towards the border of Switzerland. Grey regions indicate that no $M_{c(EMR)}$ was computed due to small earthquake sample sizes. Fig. 8(b) shows that the majority of σ_c falls between 0.1 and 0.3, whereas $\sigma_c > 0.3$ is determined outside of the network and in a small part of central Switzerland (point V). In comparison with Fig. 3(d), σ_c is generally larger than σ_P for many regions.

Sometimes temporary networks were deployed in regions of special interest. To find a meaningful comparison with the EMR approach, we investigate the performance of these networks using the PMC method. As the main temporary networks in Switzerland, we consider the 'Zeuzier' (1981–1989) (Maurer 1993; Maurer & Kradolfer 1996), the 'Nagra' (1983–2000) (Deichmann *et al.* 2000) and the 'NFP20-East' (1986–1988) (Laubscher 1994) networks. Like for the permanent network, we computed P_D for all temporary stations and M_P for each temporary network: the grid spacing is $0.05^\circ \times 0.05^\circ$ and the computation is carried out for every month in the operational period (Fig. 9). All temporary networks improved, during their operational periods, the detection capability of earthquakes very locally in comparison with the permanent network. However, note that only the Zeuzier network was installed to accurately locate microseismicity whereas the others were used for different purposes. Significant improvement can be seen only for the region in and around the Zeuzier network during the operational period. Because we want to compare the completeness estimates of both methods for the SSN and because the temporary networks were not operating during the entire period of our investigation, we are using as a conservative estimate for completeness only the Swiss permanent network, ignoring the temporary networks. However, the low completeness values in the areas of the temporary networks explain the very low $M_{c(EMR)}$ values in the areas around Basel and in the Valais. These areas reflect the temporary higher detection probabilities due to the temporary networks, however are misleading as a completeness estimate because it is dependent on the temporary networks and in fact only valid for the period of their operation.

For the comparison, we need to consider a representative parameter for the PMC method, because the PMC and EMR methods are based on two different statements. The former can be used to compute an estimate of completeness for the network at one specific point in space and time whereas using the latter method we compute a completeness estimate of an earthquake sample for a space–time volume projected onto one grid node. Therefore, we define a representative value for the PMC method based on the corresponding space–time volume used for computing $M_{c(EMR)}$. We estimate the PMC representative value as follows: (1) we use the same cylindrical volume (height of 20 km, radius of 30 km and the centre at $\boldsymbol{x}_c$) and the same period ($t_S \leq t \leq t_E$) as we do for EMR; (2) we take

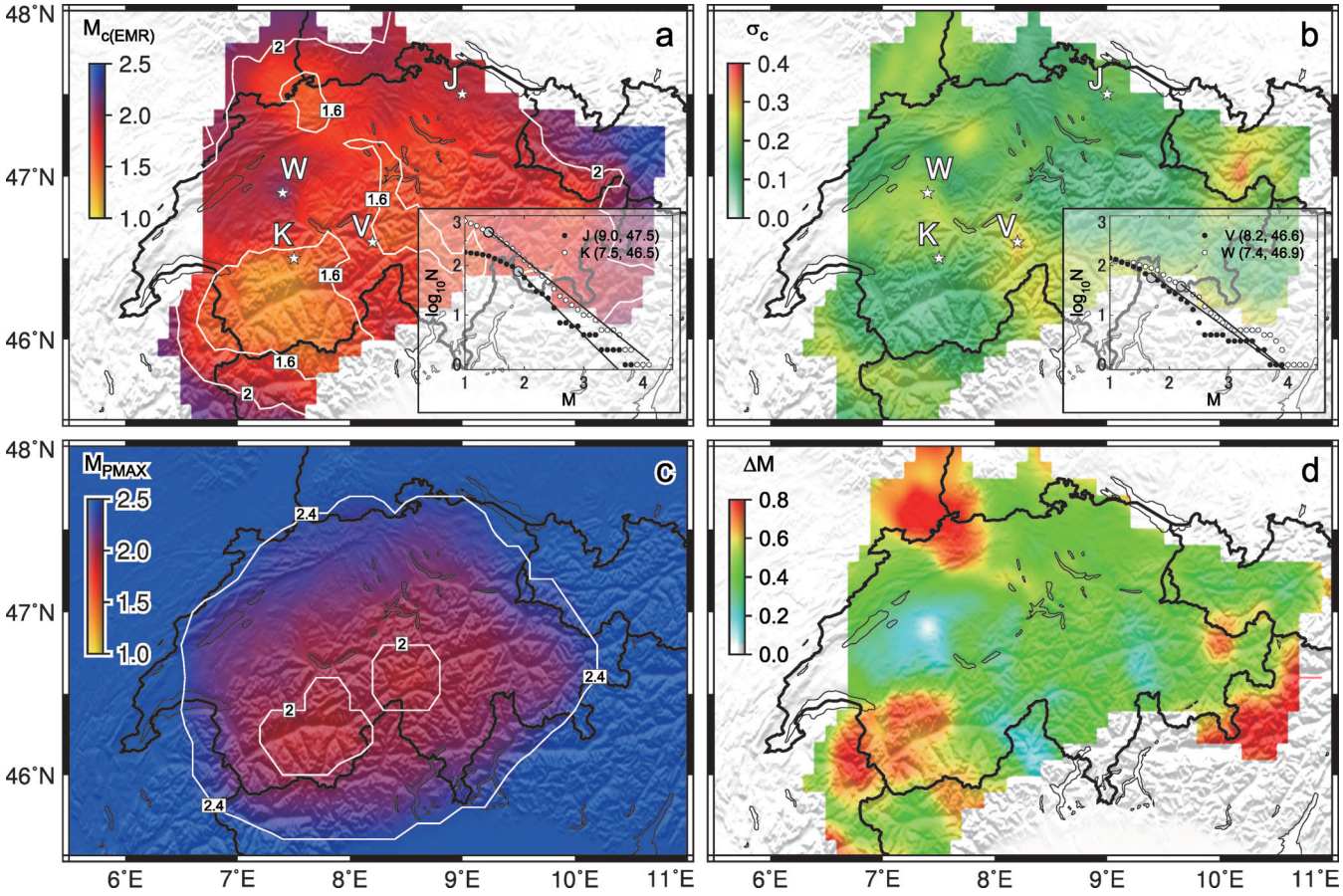

Figure 8. Maps showing (a) $M_{c(EMR)}$, (b) its uncertainty σ_c, (c) M_{PMAX} and (d) $\Delta M_{PMAX,c}$ for the period from 1983 January 1 to 2008 March 31. $M_{c(EMR)}$ and σ_c are computed for nodes where 80 or more earthquakes were sampled. The insets show frequency–magnitude distributions for four nodes, indicated by white stars. The grey circles indicate the completeness magnitude, $M_{c(EMR)}$, of each distribution.

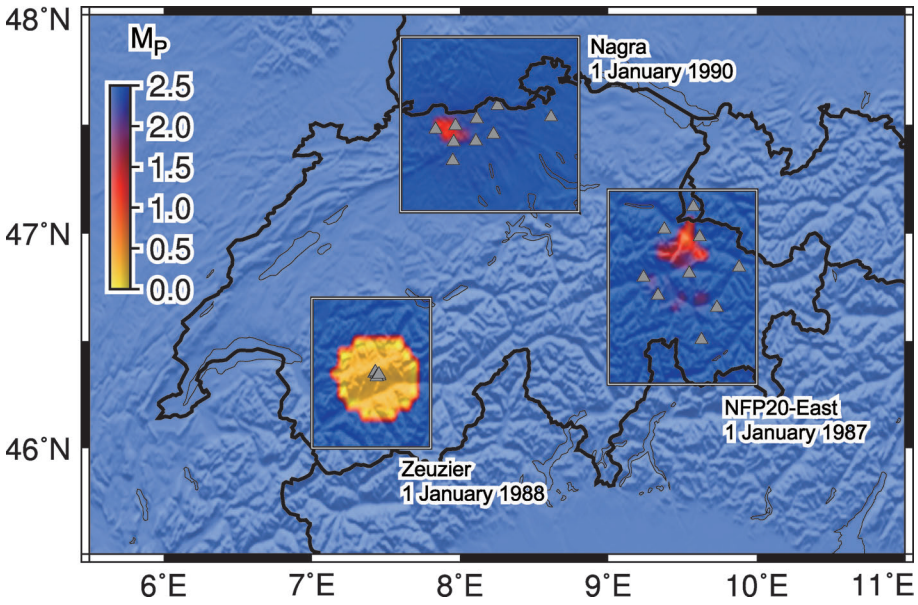

Figure 9. Map of probability-based magnitude of completeness, M_P, for temporary networks: Nagra network on 1990 January 1, NFP20-east network on 1987 January 1 and Zeuzier network on 1988 January 1. In each frame, the stations of the respective network are shown as triangles. Note that the colour scale used here is different from that used in the other figures.

the detection-probability distributions P_D for the permanent stations operating at the time t; (3) we estimate $M_P(\boldsymbol{x}_{SUB}, t)$ values for t for all possible locations $\boldsymbol{x} = \boldsymbol{x}_{SUB}$ within the cylinder, where we take a grid spacing of $\boldsymbol{x}_{SUB}$ to be $0.1^\circ \times 0.1^\circ$ and depths to be 5, 10, 15 and 20 km; (4) we take the same approach for all times in the period $t_S \leq t \leq t_E$ and (5) we take the maximum among the $M_P(\boldsymbol{x}_{SUB}, t)$ values over the period $t_S \leq t \leq t_E$ and over the cylinder. This maximum is the PMC representative and the conservative value for the volume with the centre at $\boldsymbol{x}_c$ and denoted by $M_{PMAX}(\boldsymbol{x}_c, t_S, t_E) \equiv M_{PMAX}$.

The M_{PMAX} map for 1983–2008 (Fig. 8c) shows that completeness estimates vary between $1.9 \leq M_{PMAX} \leq 2.5$ in Switzerland. The M_{PMAX} pattern and its range are most similar to those for 1983 (Fig. 5) because of the aforementioned conservative approach. Comparison with Fig. 8(a) shows that $M_{c(EMR)}$ is generally smaller than M_{PMAX}. To show the quantitative difference, we define $\Delta M_{PMAX,c} \equiv M_{PMAX} - M_{c(EMR)}$ and compute $\Delta M_{PMAX,c}$ for each volume. Fig. 8(d) shows that in Switzerland $\Delta M_{PMAX,c} \geq 0$ with most values in the range 0.1–0.5 (cyan and green) except for the point in central western Switzerland (point W) where $\Delta M_{PMAX,c} < -0.1$. $\Delta M_{PMAX,c}$ generally increases towards the borders of Switzerland, with exceptionally high values in the Valais, having $\Delta M_{PMAX,c} \geq 0.6$ (red). The temporary Zeuzier network in the Valais very often detected earthquakes with magnitudes down to $M = 0$ (Maurer 1993; Maurer & Kradolfer 1996). Because of this temporary network, EMR gives small values of $M_{c(EMR)}$ resulting in the large values of $\Delta M_{PMAX,c}$. This analysis shows the strong dependence of the EMR estimates on the particular samples, including many not resolvable effects like higher detection probabilities due to temporary networks and strongly varying completeness over time due to changing station configurations. Periods of higher recording quality will strongly dominate EMR estimates as can be seen in Fig. 8(a). Many small-magnitude events that were recorded in the most recent years let the EMR method estimate the completeness similar to the one observed for the last years (bottom row in Fig. 5) although such earthquakes were not recorded in the earlier years which were included in this computation of EMR completeness. Due to these effects, EMR often provides too optimistic and erroneous completeness estimates.

5 SUMMARY AND DISCUSSION

We examined the detection capabilities of the SSN as an example of a network in a low- to moderate-seismicity region using the recently introduced PMC method (Schorlemmer & Woessner 2008). We found the magnitude of completeness, M_P, within Switzerland to vary in the range of 1.1–2.5 for 2008 (Fig. 3c). Our analysis shows that the current network detects earthquakes of magnitude $M = 2.5$ and larger reliably for the entire Swiss territory. The temporal evolution of M_P shows a gradual improvement of the network-detection capabilities (Fig. 5 and Animation S1), highlighting the success of the network modernization (e.g. Baer *et al.* 2005).

To define M_P, we considered $P_E = 0.9999$, which could be interpreted as only one event out of 10 000 is missing in the data set. This probability is based on two assumptions: future seismicity would replicate the past seismic activity; and earthquakes are independent, identically distributed events. In reality, however, there are many confounding factors, like depth, focal mechanism, aftershock sequences and other spatial-temporal changes, which can significantly modify a station-detection probability. Moreover, external causes such as power failures or extreme meteorological events can also strongly affect the complementary probability (Q). Thus, even if contour lines of $P_E = 0.9999$ convey useful information, to avoid a misunderstanding, it is better to keep in mind that such factors and causes are not considered for this study; however, further studies should take them into account to improve the method. Only one issue among them has been addressed by Schorlemmer *et al.* (2010) who took the above external causes into account, using an example from the network of the Istituto Nationale di Geofisica e Vulcanologia (INGV).

Although systematic effects on the station-detection capabilities are not fully taken into account in this paper, we performed simple sensitivity checks on anisotropy and depth dependence of the detection capability (Fig. 4). For input data, we separately considered events situated in the NE/SW and the NW/SE quadrants of the station. Distributions of P_D are also given for two depth ranges: shallower than or equal to 7.5 km and deeper than 7.5 km. We observed that the PMC method for Switzerland provides stable estimates of P_D even if these input-data conditions change. Thus, instead of taking into account the anisotropy and depth dependence of the detection capability, we took a simple approach to use one probability obtained based on all available earthquakes for each station. Yet, an in-depth analysis of the sensitivity checks needs to be performed. Especially in regions where anisotropy in wave propagation has been detected or in more seismically active regions, we would expect to see anisotropic-detection ability and depth-dependent detectability.

Seismologists are not only interested in general maps of network detectabilities, but also in maps of the spatial distributions of missing (undetected) events. The problem to be addressed in the paper was how many events are undetected and unlisted in the SSN catalogue. We introduced an approach to estimate the number of undetected events for moderate-seismicity regions. Using events in the 2-yr period from 2006 April 1 to 2008 April 1, we found that total number of undetected earthquakes, n^u_{tot}, varies about by order of 10^9 for the studied magnitude range ($M = 0.1 - 2.5$), and n^u_{tot} generally increases with the decrease of M. We also took other three 2-yr periods to show similar feature. This demonstrates the variability of detection capabilities. Perhaps the GR relation helps to answer the number of missing events. However the GR analysis may be usually insufficiently detailed partly due to lack of sufficient earthquake data in the part of the distribution representing large but rare events as well as due to the difficulty of identifying the range over which power-law behaviour holds. Clauset *et al.* (2009) gave a similar discussion on the difficulty of power-law characterization, analysing 24 geophysical data sets. On the other hand, the maps obtained by the new method are based on a seismicity record, so our approach addresses to the problem to estimate the number of missing events.

We introduced a bootstrap approach to quantify the sensitivity of M_P to the input data. We found the standard deviation generally to be small in many regions ($\sigma_P < 0.1$, Fig. 3d), suggesting that the PMC method provides stable completeness estimates. At the current state, the estimates do not take into account systematic effects, such as day-to-night time variations, change in the routine analysis between different operators, etc. Thus, these values might be on the low end of the real uncertainty. The bootstrapping introduced is computationally intensive, and without a large computational facility it is not possible to perform this type of statistical treatment for larger study areas.

Additionally the PMC method can be used in various ways that are not restricted to estimate the completeness level.

The method allows analysing the detection capabilities, P_D, of single stations and their uncertainties, σ_D, in detecting events (Fig. 2) as well as the uncertainties of detection for the network

configuration, σ_P, (Fig. 3d). It is essential to know that many sources of data flaws exist, for example magnitude errors or event clusters, which propagate into artefacts in P_D distributions. A method proposed by Bachmann *et al.* (2007) improves the P_D determination by detecting and excluding event clusters that disturb the homogeneity of the data distributions and therefore can strongly affect P_D.

PMC can be used as a network-planning tool with scenario computations to infer the network performance for any virtual configuration (Fig. 7): this can help determining locations for future stations at low costs. However, the effectiveness of this tool needs to be investigated in more detail as it is a non-trivial task to assume a station characteristic for a new station location. Additional information like local site conditions and geological parameters need to be available. Average shear velocity down to 30 m, V_S^{30}, was suggested as a first proxy for site conditions (Wald & Allen 2007) and could be used after calibration of detection–probability distributions with V_S^{30}. Also, scenario computations for network crisis situations can be performed as discussed in Schorlemmer *et al.* (2010) for the Italian National Seismic Network.

Besides these advantages, PMC is superior to the GR-based methods in spatio-temporal resolution and probabilistic quantification of the completeness estimate.

When comparing the PMC approaches with the GR-based EMR approach (Woessner & Wiemer 2005), we found the former generally gives higher estimates than the latter with differences of 0.1–0.5 in magnitude units (Fig. 8d). These differences are explained by Schorlemmer & Woessner (2008). First, they arise because of the different data sets used: The probabilistic approach is based on phase data and station information whereas methods based on earthquake samples are using data from the end of a much larger processing chain with many choices involved. The second reason is the difference in definition of the completeness magnitude. For the GR-based approach, the completeness level is based on detecting the point of deviation from a power-law distribution of earthquake magnitudes. For the PMC approach, completeness magnitude is given as the magnitude with a very high probability (0.9999 in this study) that four or more stations have recorded the *P* wave of an earthquake.

We found systematic differences $\Delta M_{PMAX,c} > 0$ in Switzerland, mostly in the range of 0.1–0.5. Using PMC, we evaluated the performance of the SSN including permanent and temporary networks, and took, for a representative, the maximum among the M_P values over the times in 1983–2008 for each volume. The resulting pattern of maximum values (M_{PMAX}) is most similar to the M_P pattern for the 1980s before the modernization of the SSN. In contrast, the EMR-approach estimates completeness based on earthquake samples covering the period 1983–2008 for each volume. Therefore, the resulting completeness levels represent average values over this period, not sensitive to the periods where detection capability of earthquakes was lower, like in the 1980s. This explains the expected differences of $\Delta M_{PMAX,c} > 0$ and emphasizes the optimistic estimates of GR-based methods that inherently ignore periods of lower detection capability due to their averaging character.

Schorlemmer & Woessner (2008) found a better agreement for areas in southern California. They used M_P, not the maximum (M_{PMAX}) out of a time-series, and performed the comparison for a period of rather constantly high-quality recording. They also pointed out the spatial variability of the difference between EMR and PMC results with the notable Anza and Coso regions, where PMC gave significantly lower estimates. Our results also show large difference between EMR and PMC estimates in the Valais area. This is due to the effect of the temporary Zeuzier network that detected microearthquakes that were missed by the permanent network. The EMR method does not distinguish between the two contributing networks and, hence, estimates average completeness values that do not correctly characterize the permanent network. In contrary, the PMC methods can be used to compute completeness values for each single network and to assemble a complete history with high spatio-temporal resolution.

We have not yet considered the uncertainties in the basic parameters although we mimic parts of these through bootstrapping. However, magnitude and location uncertainties need to be computed correctly before propagating these through the completeness estimate methods. Probabilistic earthquake location algorithms (e.g. Lomax *et al.* 2000) provide probability density functions for location uncertainties and also include magnitude estimates. Werner & Sornette (2008) recently introduced a method to estimate magnitude uncertainties derived from earthquake catalogues. These approaches in combination with the PMC method will lead to more realistic uncertainty estimates.

There are two primary uses we foresee of the detailed space–time archive of completeness that we have constructed in this study, as follows.

(1) As a critical input for many seismicity (e.g. Husen *et al.* 2007) and probabilistic seismic hazard (PSHA) studies. This is particularly useful for regions of moderate to low seismicity, where users interested in a complete catalogue cannot readily cut the catalogue at a very conservative choice of M_c, because the remaining seismicity rates would be too low for a reliable estimation of the local activity rates. The current generation of PSHA for Switzerland (Wiemer *et al.* 2008), for example, uses magnitudes as small as 1.5 for rate estimation. The next generation of PSHA for Switzerland may thus make use of the M_P model of this study.

(2) As a feedback for network operators on the performance of their network, and as a planning tool for future upgrades to the network. The SED plans to integrate automated monitoring of PMC- and EMR-based completeness as one integral part of routine quality assessment. It also plans to use the virtual station approach (Fig. 7) as a planning tool to optimize the placement of future stations.

All input data, codes and results are published on the website www.completenessweb.org for free download.

ACKNOWLEDGMENTS

The authors thank the SED for earthquake and station catalogues and C. Bachmann, M. Baer, A. Christophersen, J. Clinton, N. Deichmann and S. Husen for their valuable comments. We would also like to acknowledge the Associate Editor (Y. Ben-Zion) and two very helpful reviews from Y. Y. Kagan and K. Felzer. In particular, we want to thank the open-source community for the Linux operating system and the many programs used in this study. Figures were created using Generic Mapping Tools (Wessel & Smith 1995). The work was supported by EC-FP6-Project SAFER contract 036935, EC-Project NERIES contract 026130, USGS NEHRP grant 07HQR0034 and NSF-EAR-0738785 grant, and Special Project for Earthquake Disaster Mitigation in Tokyo Metropolitan Area from the Ministry of Education, Culture, Sports, Science and Technology of Japan.

REFERENCES

Bachmann, C., Schorlemmer, D., Woessner, J. & Wiemer, S., 2005. Probabilistic estimates of monitoring completeness of seismic networks

(abstract), *EOS Trans. Am. Geophys. Un.,* **86**(52), Fall Meet. Suppl., Abstract S33–0304.

Bachmann, C., Schorlemmer, D., Kissling, E. & Oppenheimer, D., 2007. Probabilistic magnitude of completeness of the Northern Californian Seismic Networks—Strategies for reducing data flaws, *Seismol. Res. Lett.,* **78**(2), 292.

Baer, M. *et al*., 2005. Earthquakes in Switzerland and surrounding regions during 2004, *Eclogae geol. Helv.,* **98**(3), 407–418.

Braunmiller, J., Deichmann, N., Giardini, D., Wiemer, S. & the SED Magnitude Working Group, 2005. Homogeneous moment-magnitude calibration in Switzerland, *Bull. seism. Soc. Am.,* **95**(1), 58–74.

Clauset, A., Shalizi, C. R. & Newman, M. E. J., 2009. Power-law distributions in empirical data, *SIAM Rev.,* **51**(4), 661–703.

Deichmann, N., Ballarin Dolfin, D. & Kastrup, U., 2000. Seismizität der Nord- und Zentralschweiz, *Technischer Bericht,* **00–05**, ISSN 1015–2636.

Efron, B., 1979. Bootstrap methods: another look at the Jackknife, *Ann. Statist.,* **7**(1), 1–26.

Fäh, D. *et al*., 2003. Earthquake catalogue of Switzerland (ECOS) and the related macroseismic database, *Eclogae geol. Helv.,* **96,** 219–236.

Gutenberg, B. & Richter, C., 1944. Frequency of earthquakes in California, *Bull. seism. Soc. Am.,* **34,** 185–188.

Husen, S., Bachmann, C. & Giardini, D., 2007. Locally triggered seismicity in the central Swiss Alps following the large rainfall event of August 2005, *Geophys. J. Int.,* **171,** 1126–1134.

Kradolfer, U., 1984. Magnitudenkalibrierung von Erdbebenstationen in der Schweiz, Swiss Federal Institute of Technology Zurich, *Diploma thesis*. ETH Zurich, Zurich, Switzerland.

Laubscher, H., 1994. Deep structure of the central Alps in the light of recent seismic data, *Geol. Rundsch,* **83,** 237–248.

Lomax, A., Virieux, J., Volant, P. & Berge, C., 2000. Probabilistic earthquake location in 3D and layered models, in *Advances in Seismic Event Location,* pp. 101–134, eds Thurber, C. H. & Rabinowitz, N., Kluwer Academic Publishers, Dordrecht/Boston/London.

Matsumura, S., 1984. Evaluation of detection capability of microearthquakes for an observational network –The Kanto-Tokai observational network of the National Research Center for Disaster Prevention-, *ZISHIN (J. seism. Soc. Japan),* **37,** 475–489 (in Japanese with English abstract).

Maurer, H., 1993. Seismotectonics and upper crustal structure in the western Swiss Alps, Swiss Federal Institute of Technology Zurich, *Doctor dissertation*. ETH Nr. 10268, Zurich, Switzerland.

Maurer, H. & Kradolfer, U., 1996. Hypocentral parameters and velocity estimation in the western Swiss Alps by simultaneous inversion of P- and S-wave data, *Bull. seism. Soc. Am.,* **86**(1A), 32–42.

Morandi, M. T. & Matsumura, S., 1991. Update on the examination of the seismic observational network of the National Research Center for Disaster Prevention (NIED) –Detection capability and magnitude correction, in *Report on the National Research Institute for Earth Science and Disaster Prevention No. 47 (March 1991),* pp. 1–18, The National Research Institute for Earth Science and Disaster Prevention, Ibaraki, Japan.

Nanjo, K. Z., Enescu, B., Shcherbakov, R., Turcotte, D. L., Iwata, T. & Ogata, Y., 2007. Decay of aftershock activity for Japanese earthquakes, *J. geophys. Res.,* **112,** B08309, doi:10.1029/2006JB004754.

Ogata, Y. & Katsura, K., 1993. Analysis of temporal and spatial heterogeneity of magnitude frequency distribution inferred from earthquake catalogs, *Geophys. J. Int.,* **113,** 727–738.

Papanastassiou, D. & Matsumura, S., 1987. Examination of the NRCDP's (The National Research Center for Disaster Prevention) seismic observational network as regards I. Detectability-locatability, II. Accuracy of the determination of earthquake source parameters, in *Report on the National Research Center for Disaster Prevention No. 39 (March 1987),* pp. 37–65, The National Research Center for Disaster Prevention Science and Technology Agency, Ibaraki, Japan.

Schorlemmer, D. & Woessner, J., 2008. Probability of detecting an earthquake, *Bull. seism. Soc. Am.,* **98**(5), 2103–2217, doi:10.1785/0120070105.

Schorlemmer, D., Wiemer, S. & Wyss, M., 2005. Variations in earthquake-size distribution across different stress regimes, *Nature,* **437,** 539–542.

Schorlemmer, D., Mele, F. & Marzocchi, W., 2010. A completeness analysis of the National Seismic Network of Italy, *J. geophys. Res.,* **115,** B04308, doi:10.1029/2008JB006097.

Wald, D. J. & Allen, T. I., 2007. Topographic slope as a proxy for seismic site conditions and amplification, *Bull. seism. Soc. Am.,* **97**(5), 1379–1395.

Werner, M. J. & Sornette, D., 2008. Magnitude uncertainties impact seismic rates estimates, forecasts and predictability experiments, *J. geophys. Res.,* **113,** B08302, doi:10.1029/2007JB005427.

Wessel, P. & Smith, W. H. F., 1995. New version of the Generic Mapping Tools released, *EOS, Trans. Am. geophys. Union,* **76,** 329.

Wiemer, S. & Wyss, M., 2002. Mapping spatial variability of the frequency-magnitude distribution of earthquakes, *Adv. Geophys.,* **45,** 259–302.

Wiemer, S., Giardini, D., Fäh, D., Deichmann, N. & Sellami, S., 2008. Probabilistic seismic hazard assessment of Switzerland: best estimates and uncertainties, *J. Seismol.,* **13**(4), 449–478, doi:10.1007/s10950-008-9138-7.

Woessner, J. & Wiemer, S., 2005. Assessing the quality of earthquake catalogs: estimating the magnitude of completeness and its uncertainties, *Bull. seism. Soc. Am.,* **95**(4), 684–698.

SUPPORTING INFORMATION

Additional Supporting Information may be found in the online version of this article:

Animation S1. Temporal evolution of M_P maps since 1983 January 1. Each snapshot is created for the times $t =$ the first day of every month shown in the upper right corner. Operating stations are indicated by triangles. Installation and decommission of stations are shown by squares and crosses, respectively.

Please note: Wiley-Blackwell are not responsible for the content or functionality of any supporting materials supplied by the authors. Any queries (other than missing material) should be directed to the corresponding author for the article.